



Sealing analysis of face-milled surfaces based on high definition metrology

Yaxiang Yin^{a,b}, Shichang Du^{a,b,*}, Yiping Shao^c, Kun Wang^{a,b}, Lifeng Xi^{a,b}

^a State Key Lab of Mechanical System and Vibration, Shanghai Jiao Tong University, Shanghai, 200240, China

^b School of Mechanical Engineering, Shanghai Jiao Tong University, No. 800 Dongchuan Road, Shanghai, 200240, China

^c College of Mechanical Engineering, Zhejiang University of Technology, Hangzhou, China

ARTICLE INFO

Keywords:

Sealing analysis
Face-milling
Cylinder head gaskets
Channel directions
High definition metrology

ABSTRACT

Leakage is always a concern in the interface between the cylinder block and the head. Nowadays, sealing of this interface is almost exclusively achieved by multi-layer steel head gaskets. However, it is not only the gasket's quality that is responsible for perfect sealing. An equally important role is played by the surface topography of the mating surfaces. The top surface of the cylinder block and the bottom surface of the cylinder head are machined by face-milling and present periodic tool marks features. Based on the surface topography measured by high definition metrology, this paper presents a novel sealing analysis method to evaluate the sealing performance of the critical topography region around the combustion chambers. The method consists of three modules: tool paths or channels reconstruction, sealing region segmentation based on channels' directions, and sealing analysis on sealing regions with different channel directions. An engineering case demonstrates the sealing analysis procedures and verifies the effectiveness of the sealing analysis method. The analysis of 12 ring-shaped sealing regions found that channels' directions do have a significant impact on surfaces' sealing properties. Circumferential channels or paths are advantageous for surface sealing, while radial channels are prone to leakage.

1. Introduction

Leakage is always an important concern in the interface between the cylinder block and the head. Once leakage happens, it will cause engine power reduction, engine overheating, and even engine failures. Fig. 1 shows a cylinder head with a leakage problem, the leakage area is contaminated by carbon deposition and blackening marks. The red circles in Fig. 1 outline some marks of the leakage and the sealing of this interface is a failure.

The sealing of the interface between the cylinder block and the head is mainly influenced by the gasket, the mating surfaces' topography and the bolt torque [1]. Increasing high ignition pressures and temperatures lead to high stresses for head gaskets. The multi-layer steel (MLS) gasket is developed to adapt to the trend of engine design and offers higher sealing potential [2,3]. A typical 3-layer MLS head gasket with a top layer, a stopper layer and a bottom layer is shown in Fig. 2. Beads around combustion chambers and oil/coolant passages increase the local sealing pressure (macro sealing), whilst full-surface or partial elastomer coatings provide additional sealing tightness (micro sealing) [4,5].

Despite a carefully designed gasket, the leakage can still occur during

practical operation due to numerous possible causes. In total, seven different types of media leakage could occur with MLS head gaskets, and they are outlined in Fig. 3. Among the seven types of leakage, the gas leakage between combustion chambers is most harmful and it is also a difficult leakage problem to overcome. Once the high-temperature combustion gas blows by the gasket surface, the gasket will be destructed and lose its sealing capacity soon. Therefore, this paper mainly focuses on the sealing regions around combustion chambers.

The sealing performance of the interface between the cylinder block and the head not only relies on the gasket's quality but also depends on the surface qualities of the cylinder head and engine block. The quality of the surface finish of the two mating surfaces is a decisive factor for sealing results [6]. However, the surface topography of the mating surfaces is affected by many processes factors and consists of multiscale machining errors. To ensure the sealing pressures around combustion chambers are higher than the highest ignition pressure, the torque of the bolt is several times of theoretical values in engineering practice. However, too much bolt torque not only increases the sealing pressures but also enlarges the distortion of cylinder bores and reduces the elastic recovery capacity of gaskets. It is desired to lower the torque of the bolts

* Corresponding author. State Key Lab of Mechanical System and Vibration, Shanghai Jiao Tong University, Shanghai, 200240, China.

E-mail addresses: yaxiang@sjtu.edu.cn (Y. Yin), lovbin@sjtu.edu.cn (S. Du), syp123gh@zjut.edu.cn (Y. Shao), wangkun1224@sjtu.edu.cn (K. Wang), lfxi@sjtu.edu.cn (L. Xi).

<https://doi.org/10.1016/j.precisioneng.2021.08.020>

Received 24 June 2021; Received in revised form 26 August 2021; Accepted 27 August 2021

Available online 1 September 2021

0141-6359/© 2021 Elsevier Inc. All rights reserved.

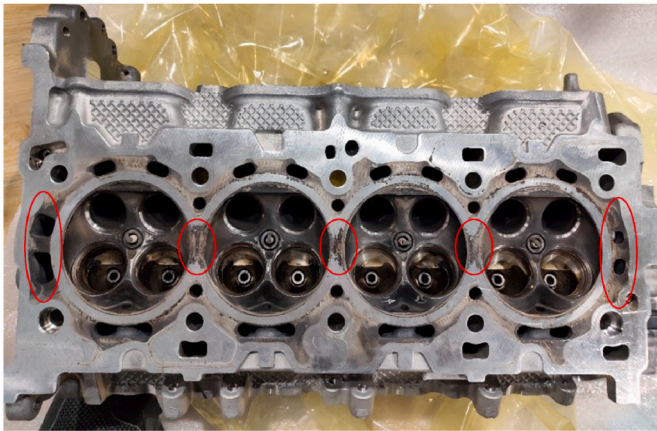


Fig. 1. A cylinder head with the leakage problem.

without reducing sealing performance.

In general, the better the surface finish, the lower the torque required to achieve sealing. However, the relationship between surface topography and its sealing capacity is unclear. Understanding the sealing properties of surface topographies is of great importance for gasket optimum design and reducing the required torque of bolts. Many efforts have been taken to clarify the sealing capacity of rough surface topographies.

Persson et al. proposed a critical junction theory to estimate the leak rate of static seals based on fractal geometry and percolation theory [7–9]. Bottiglione et al. extended the critical junction theory by considering multiple leakage channels to explain the leakage in flat seals [10,11]. Effective-medium theory of leak rates was developed further by Persson et al. to explain the leakage mechanism of rubber seals and this theory is in good agreement with experimental data [12]. Pérez-Ràfols

et al. presented a model to study the leakage through metal-to-metal seals accounting for both the surface waviness (spiral grooves) and roughness [13]. Lorenz and Persson found that the leak rate of seals depends sensitively on the skewness in the surface height probability distribution through critical-junction theory analysis and experimental data verification [14]. Ledoux et al. researched the impact of modal contents of surface defects on flat seal efficiency and found that the common roughness specification is not a relevant one to ensure sealing performance [15]. Hao et al. investigated the effect of surface topography parameters (including surface roughness, circumferential waviness and radial taper) on the liquid film sealing performance, and found that waviness is the most significant influencing factor [16]. Liu et al. investigated the effect of the topography of face-milled surfaces on adhesive sealing performance and found that the surface roughness could enhance the contact area between adhesive and joint machined surfaces, and also adhesive strength [17]. Zhang et al. proposed an approach to calculate leak channels and leak rates based on measured surface topography and finite element method [18]. Malburg considered the adaptability of gaskets and proposed to simulate the contact distribution by morphological closings on waviness profiles [19]. Later, such thought was extended to three-dimensional cases by Shao et al. and a leakage monitoring method based on measured surface topography was proposed [20,21].

Most researches about leakage mechanism are built on an assumption of isotropic surface topography. However, engineering surfaces produced by different machining methods present different characteristics. Face-turning and face-milling are two general manufacturing technologies to produce smooth surfaces with anisotropic surface topography. And the most important anisotropy of the surface topography is produced by the cutting tool trajectories, which are rarely emphasized in current literature. Deltombe et al. compared two kinds of surface finishing of rods used for sealing and found that a repeated pattern perpendicular to the leaking direction could enhance sealing

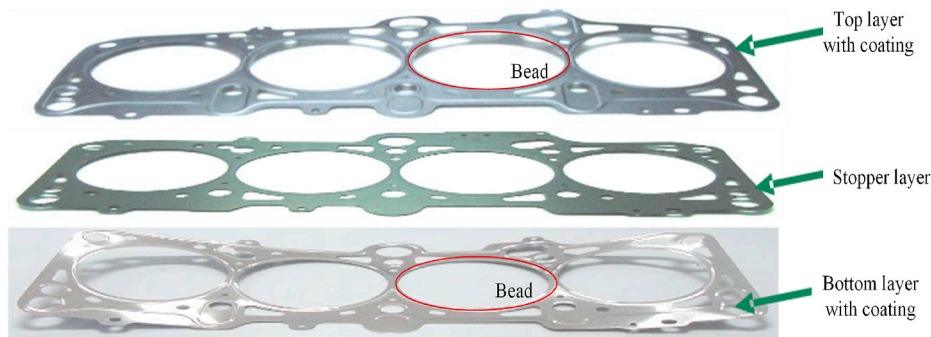
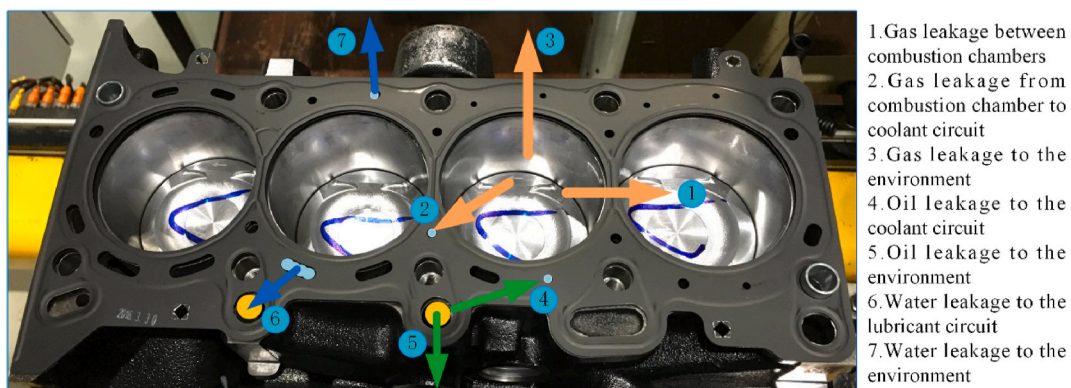


Fig. 2. A typical 3-layer MLS head gasket.



1. Gas leakage between combustion chambers
2. Gas leakage from combustion chamber to coolant circuit
3. Gas leakage to the environment
4. Oil leakage to the coolant circuit
5. Oil leakage to the environment
6. Water leakage to the lubricant circuit
7. Water leakage to the environment

Fig. 3. Seven types of media leakage on head gaskets.

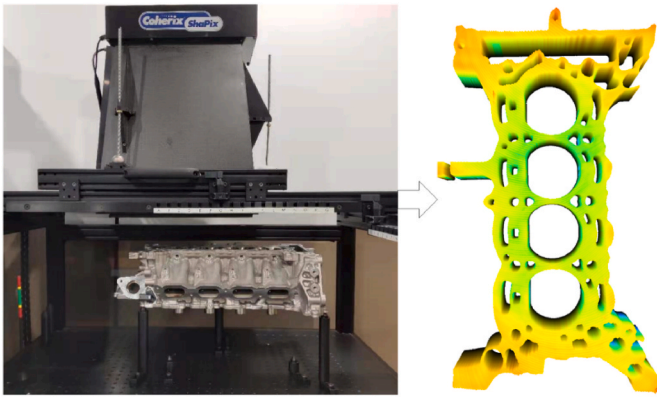


Fig. 4. Measurement by HDM

performance [22]. Yang et al. investigated the relationship between the percolation threshold (equals to one minus critical contact area percentage) and the rough surface anisotropy and found that surface anisotropy has a significant impact on the percolation threshold [23]. Liao et al. proposed a leakage model of metallic static seals based on the micromorphology of face-turned surfaces [24]. The experiment data and leakage model both found that the magnitude of the radial leakage is much greater than that of the circumferential leakage rate when the contact pressure is small. And with the increase of contact pressure, the leakage will transit from radial leak to circumferential leak. Robbe-Valloire and Prat analyzed the sealing properties of face-turned surfaces' topography based on the waviness-motif method [25]. The cutting tool trajectories play a significant role in leakage estimation since radial leakage is quite different from circumferential leakage. The same analysis logic is also appropriate for face-milled surfaces. The top surface of cylinder blocks and bottom surface of cylinder heads are two key sealing surfaces produced by face-milling and face severe leakage risks. The motivation of this paper is to present a model for sealing analysis of face-milled surfaces and research the impact of tool paths' directions on sealing properties.

The precondition of sealing analysis of face-milled surfaces is to obtain the topography of the full surfaces. In recent years, a non-contact measurement instrument named high definition metrology (HDM) is developed to fulfill the demand of measuring large plane surfaces with full resolution. Based on the principle of laser holographic interference, HDM could generate millions of data points for an engineering surface. The HDM equipment and an engine head measured by HDM are shown in Fig. 4. Based on this novel measurement platform, several studies about the three-dimensional surface topography have been developed including surface error evaluation [26,27], surface segmentation [28] and leakage path exploration [21,29]. A comprehensive study on surface quality control and application using high definition metrology is included in a recently published book [30].

With the newly developed measurement platform, the main contribution of this paper is to propose a sealing analysis framework for face-milled surfaces' topography considering the cutting tool trajectories. The topography around the combustion chamber is sampled first according to the gasket bead width. The tool paths or channels are reconstructed by a newly developed surface segmentation methodology [28]. The critical region around the combustion chamber is divided into two kinds of sub-regions based on channels' directions, and each sub-region is analyzed by a contact simulation and sealing analysis method. The contact area percentage threshold (*CAPT*, the minimum contact area required to stop leakage) is found by a binary searching algorithm.

The remainder of this paper is organized as follows. The detailed sealing analysis workflow is presented in Section 2. In Section 3, a case study demonstrates the sealing analysis procedures and draws some practical engineering conclusions. Section 4 summarizes this study and discusses the future research directions.

2. Methodology

An overview of the sealing analysis method is shown in Fig. 5. It mainly consists of the following three modules.

Module 1: The medium-scale component of face-milled surfaces' topography consists of periodic tool marks produced by tool trajectories.

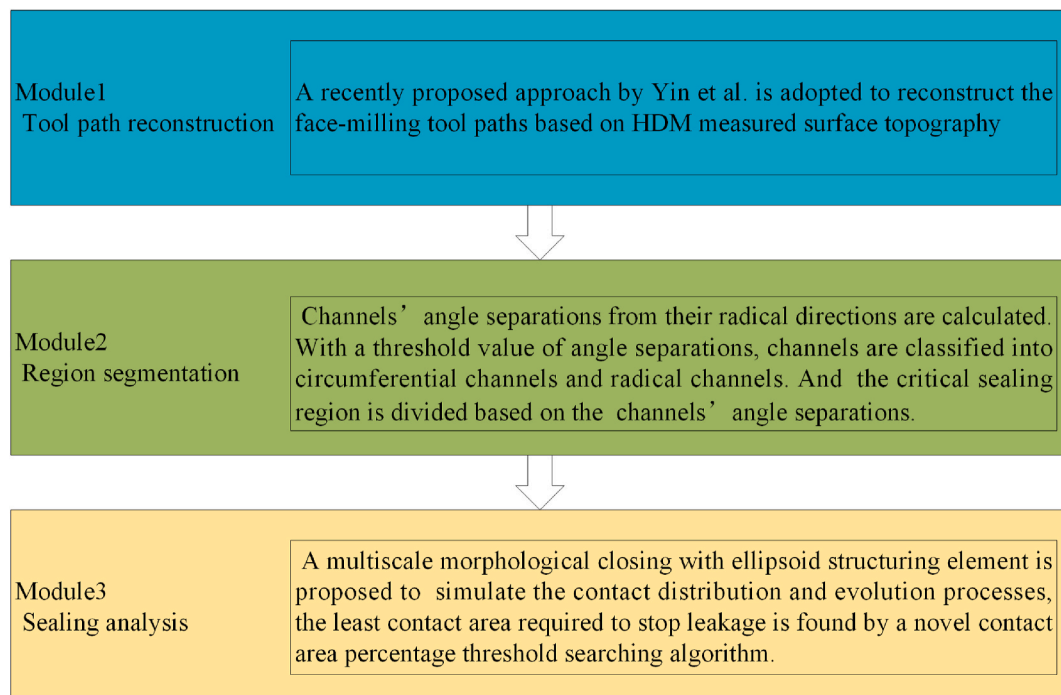


Fig. 5. Framework of the sealing analysis of face-milled surfaces.

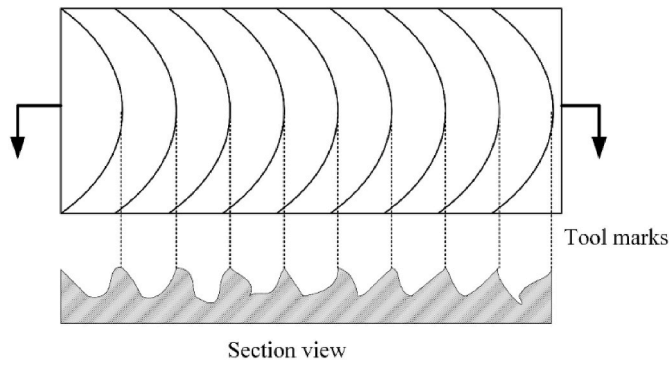


Fig. 6. Surface appearance of the face-milled workpiece.

The deep grooves of each tool path could be considered as potential leakage channels. To reconstruct the tool paths or channels, a recently developed surface segmentation method proposed by Yin et al. [28] is adopted to detect the potential leakage channels.

Module 2: Potential leakage channels could be classified into radial channels and circumferential channels according to their angle separations from their radial directions. An angle separation threshold value is

found to distinguish circumferential channels from radial channels. Based on different orientations of channels, a region segmentation method is proposed to divide the critical sealing topography into four distinct sub-regions.

Module 3: For each sub sealing region, a three-dimensional morphological closing operation is adopted to simulate the contact distribution and evolution on the interface between cylinder gaskets and face-milled surfaces. Different from the traditional ball or flat structuring elements, a novel ellipsoid structuring element is proposed to speed up the closing operations and reduce the end effect of morphological operations. To study the influence of channel directions on topography sealing properties, a contact area percentage threshold (CAPT) searching algorithm is proposed. It could find the minimum contact area required to stop leakage for sealing regions with different channel directions.

2.1. Tool paths reconstruction

Face-milled surfaces present distinct periodic tool marks, as shown in Fig. 6. In this paper, the local peaks of milled surface topography are called tool marks (the dotted lines in Fig. 6 present the concept of tool marks). And the local grooves are considered as potential leakage

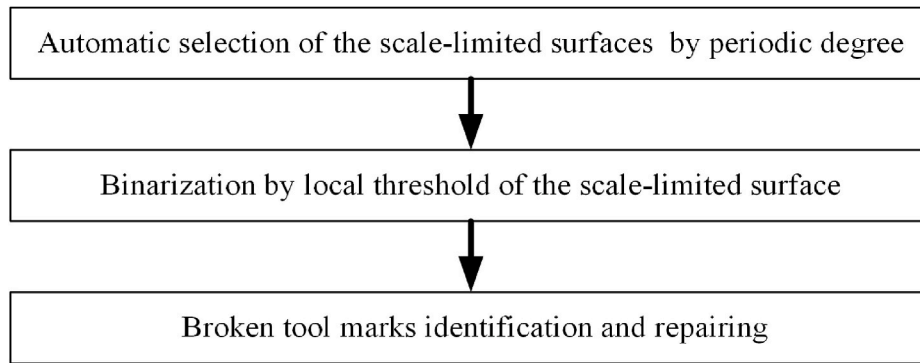


Fig. 7. The workflow to reconstruct tool paths.

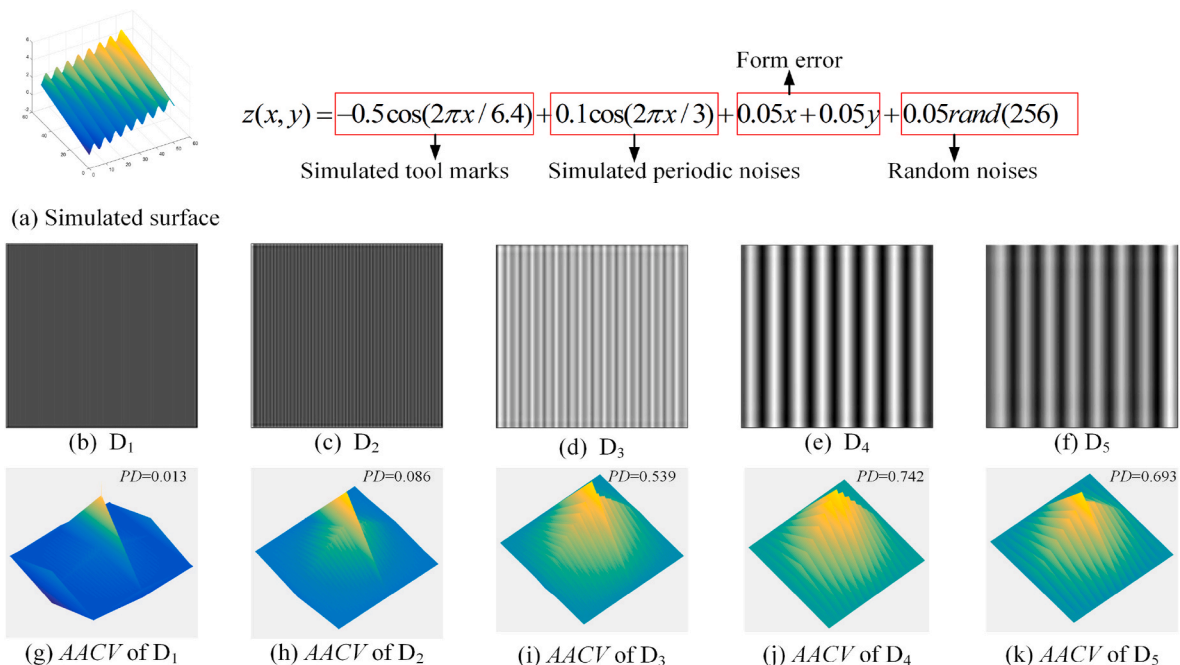


Fig. 8. Example of scale-limited surfaces selection by periodic degree.

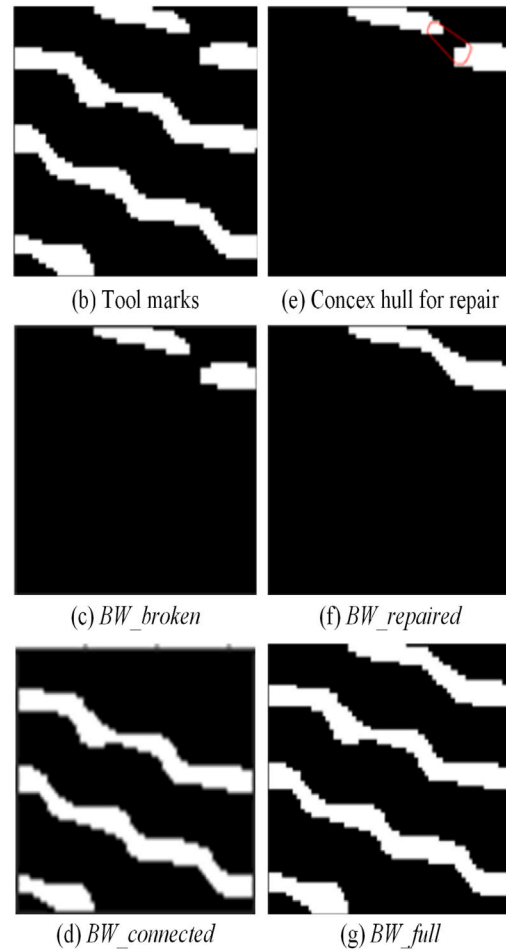
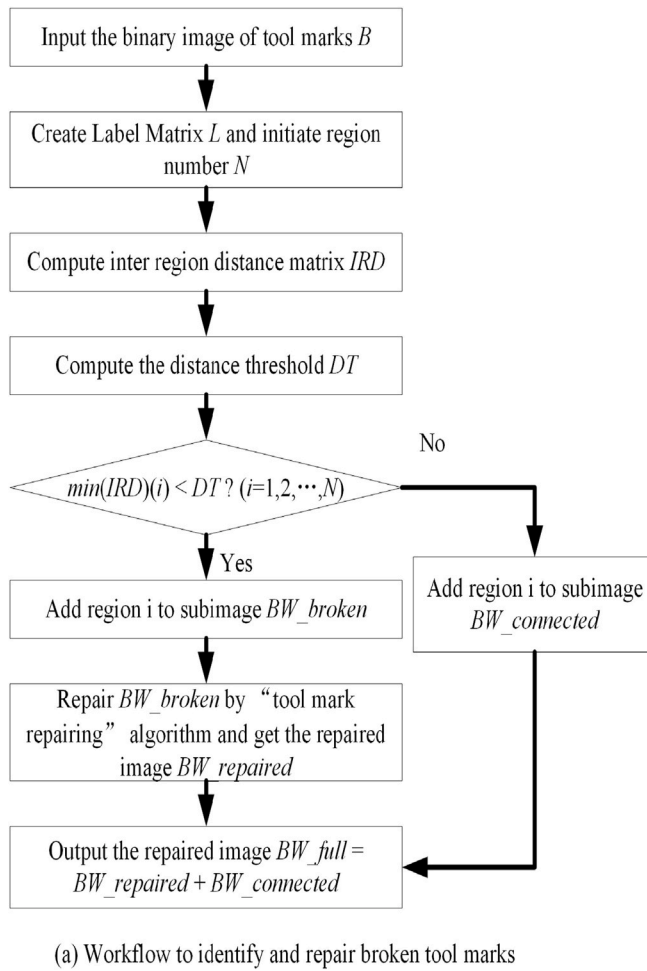


Fig. 9. Workflow and an example of broken tool marks identification and repairing.

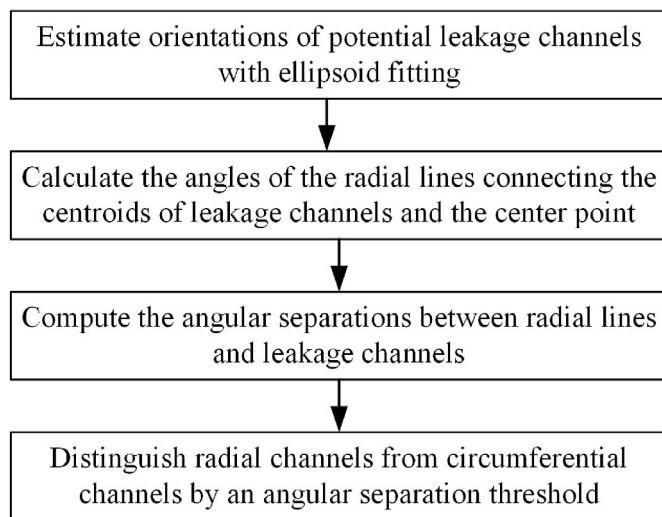


Fig. 10. An angle thresholding method to classify potential leakage channels.

channels. Due to multiple processing errors, tool marks and grooves are contaminated by other machining errors and far from ideal shapes. To clarify the relationship between face-milled surface topography and its sealing performance, the first step is to reconstruct the tool paths from measured surface topography. Local grooves and tool marks are a pair of opposite concepts. For a reversed face-milled surface topography, the

tool marks changed into local grooves and local grooves become tool marks. So, the first step only focuses on tool marks reconstruction, and the local grooves could be reconstructed in the same manner using the reversed topography. A recently proposed face-milled surface topography segmentation methodology in the previous research [28] is adopted to reconstruct the tool marks and local grooves. A flowchart of the approach is shown in Fig. 7, and the detailed procedures are reviewed as follows:

Step1: Since tool marks are mixed with other machining errors, the milled surface topography must be filtered to get the scale-limited surface (filtered surface component with certain cutoff wavelengths) that shows the tool marks most clearly. Because the tool marks are generated by periodic rotational motion, the scale-limited surface mainly consists of tool marks must present high periodic features. Therefore, a new concept called “periodic degree” is proposed to select the scale-limited surface with the highest periodic degree. Periodic degree (PD , see equation (1)) is defined as the ratio of the secondary peak height (H_{sp}) to the highest peak height (H_{hp}) on the areal auto-covariance function (AACV, see equation (2)) map. To avoid noisy fake peaks, the “peak” is defined as any point that rises above forty-eight nearest neighbors on the AACV map.

$$PD = \frac{H_{sp}}{H_{hp}} \quad (1)$$

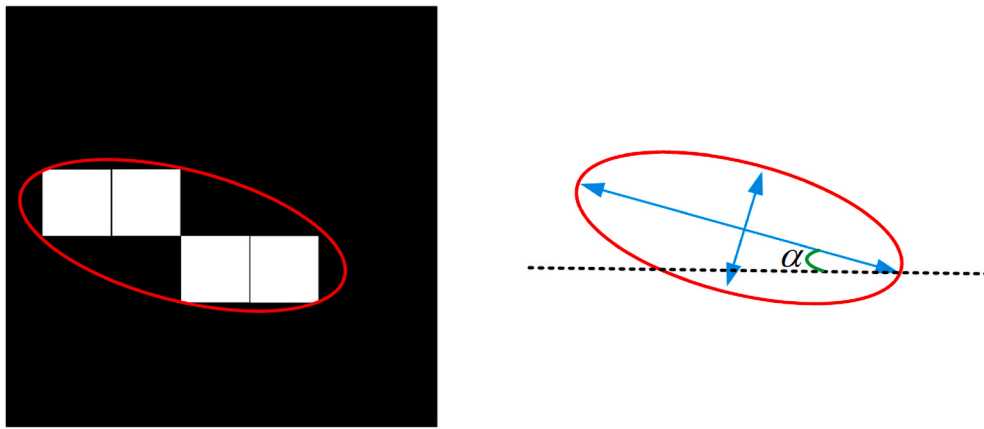


Fig. 11. Orientation estimation with ellipsoid fitting.

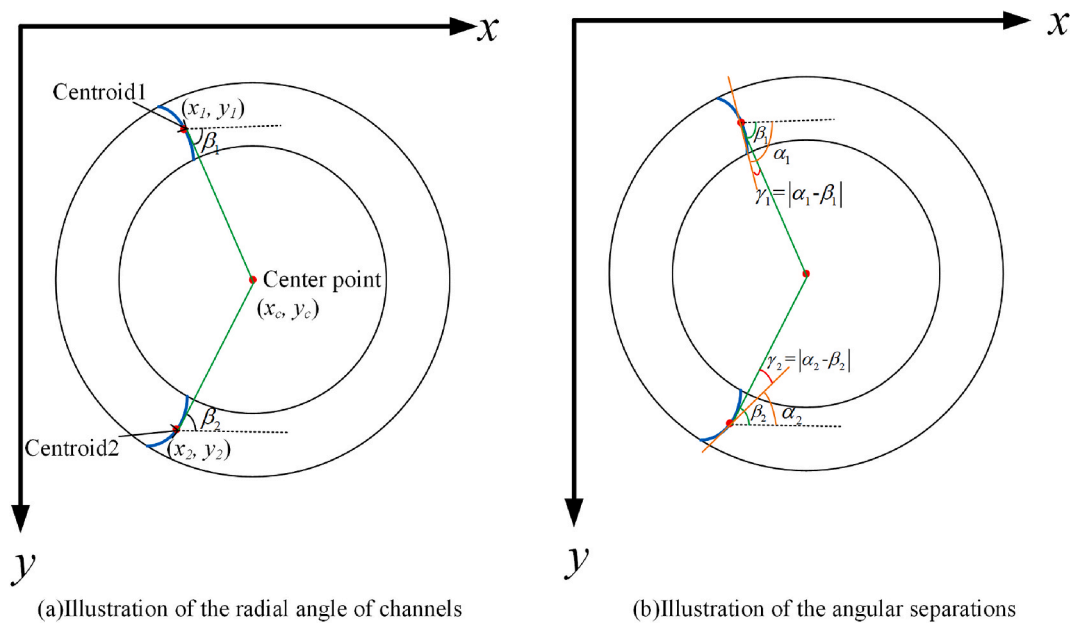


Fig. 12. Illustration of the radial angles and the angular separations.

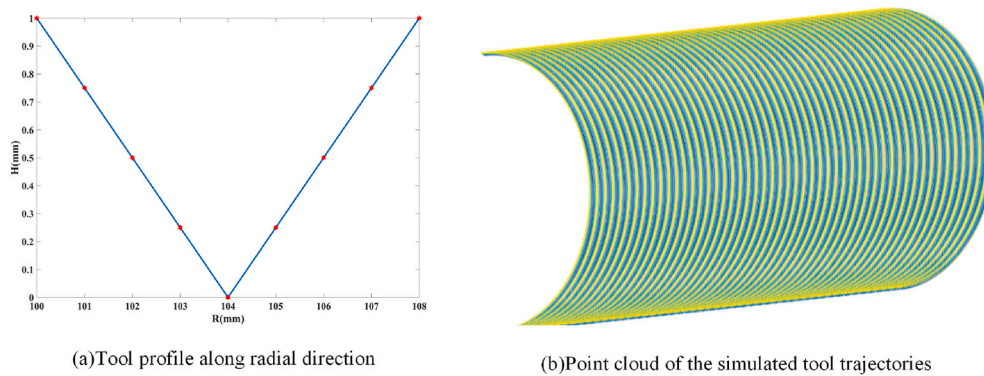


Fig. 13. The tool profile and the corresponding simulated tool trajectories.

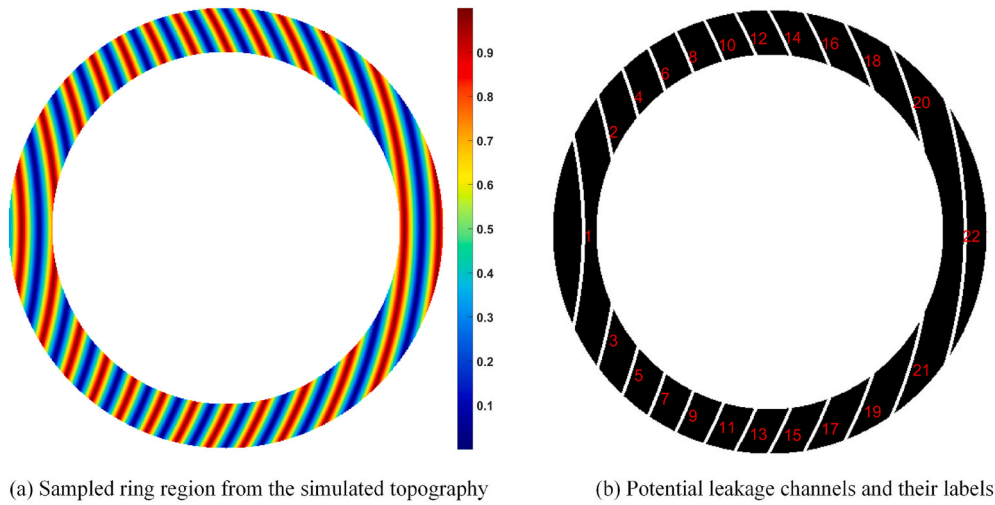


Fig. 14. A sampled ring-shaped topography and the potential leakage channels.

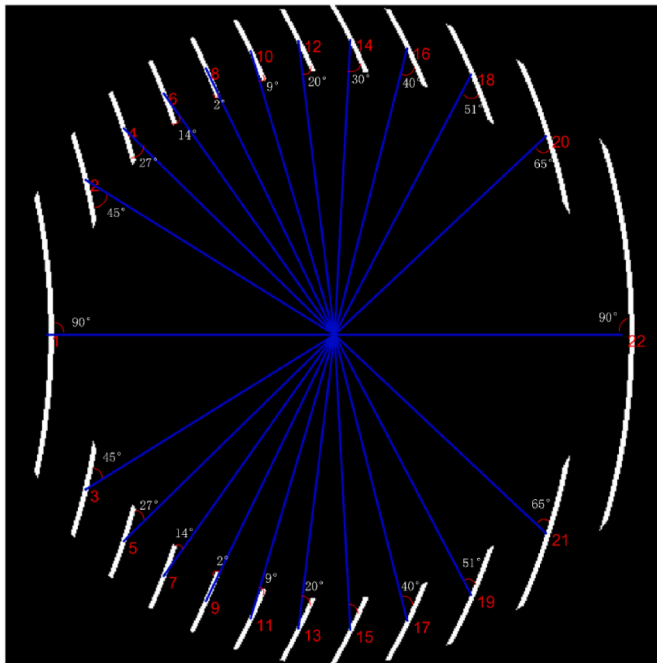


Fig. 15. Angular separations of the potential leakage channels with radial directions.

$$AACV(j', i') = \frac{1}{n_x \times n_y} \sum_{i=1}^{n_x-i'} \sum_{j=1}^{n_y-i'} z(j, i)z(j+j', i+i'), 0 \leq j' \leq n_y - 1, 0 \leq i' \leq n_x - 1 \quad (2)$$

A simulated surface (shown in Fig. 8(a)) containing form error, periodic noises and random noises is decomposed by biorthogonal wavelets in a recursive form of $A_i = A_{i+1} + D_{i+1}$ (define $D_i = D_i^H + D_i^V + D_i^D$ and A_0 is the original surface). The scale-limited surfaces $D_1 \sim D_5$ are shown in Fig. 8(b) ~ (f), and the corresponding AACV plots are shown in Fig. 8(g) ~ (k) respectively. By periodic degree calculation, the scale-limited surface D_4 is selected for tool marks extraction as expected.

Step2: A local thresholding method is applied to the selected scale-limited surface to separate tool marks from the background. Local threshold has the advantage of adapting surface fluctuations since it is determined only by the properties of a small neighborhood of a point.

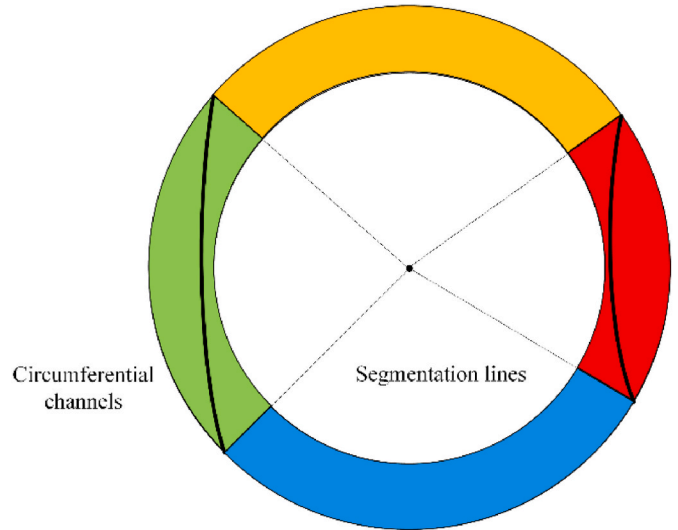


Fig. 16. The principle of sealing region segmentation.

Let σ_{xy} and m_{xy} denote the standard deviation and mean value of the heights of adjacent points centered at (x, y) . The local threshold is defined as equation (3), where a and b are nonnegative constants.

$$T_{xy} = a\sigma_{xy} + bm_{xy} \quad (3)$$

Step 3: Due to irregularities of real surfaces, tool marks may be unconnected after thresholding. The size of the breakage gaps is usually smaller than the distance of adjacent tool marks, the inter-region distance (IRD) matrix could be used to identify broken tool marks. The element $IRD(i, j)$ represents the minimum distance between the region labeled i and j , and it is defined as equation (4). The maximum of $\min(IRD)$ (minimum column by column) is approximately the distance between adjacent tool marks. The adaptive distance threshold DT could be set to a proportion of $\max(\min(IRD))$ according to engineering experiences, as equation (5) expresses.

$$IRD(i, j) = \min \sqrt{(x_p^i - x_q^j)^2 + (y_p^i - y_q^j)^2} \quad (p = 1, 2, \dots, N_i, q = 1, 2, \dots, N_j, i \neq j) \quad (4)$$

$$DT = C \times \max(\min(IRD)) \quad (5)$$

The identified broken tool marks could be repaired by the repairing

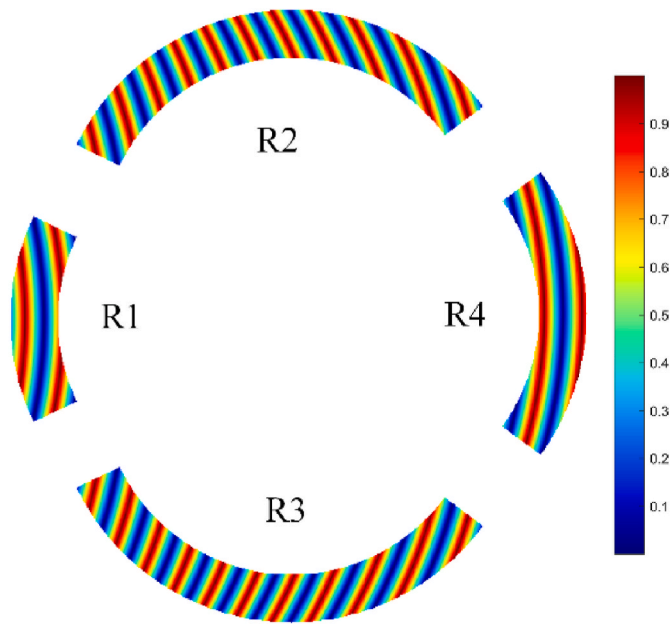


Fig. 17. The sealing region segmentation result of the simulated surface.

algorithm (for details, see Ref. [28]). The workflow to identify and repair broken tool marks is illustrated in Fig. 9(a), and an example of the identification and repairing processes is shown in Fig. 9(b) ~ (g).

2.2. Sealing region segmentation

The deep grooves along with tool paths are potential leakage channels. Radial channels face severe leakage risks, while circumferential channels could prevent leakage with little contact area. To reveal this intrinsic different effect brought by the different orientations of channels, an angle-based classification algorithm is proposed to distinguish such two kinds of channels. The procedures are outlined in Fig. 10 and described as follows:

Step1: The shape of potential leakage channels is close to a straight line. And the orientation of channels could be estimated by the angle between the x-axis and the major axis of the ellipse that has the same second-moments as the channel region. The orientation value is determined by the acute angle, ranging from -90 to 90° . Fig. 11 illustrates an example of the orientation of the channel. The left side of the figure shows a channel region and its corresponding fitting ellipse. The right side shows the same ellipse with the solid blue lines representing the axes, and the orientation is the angle α between the horizontal black

dotted line and the major axis. Note that α is a negative value in Fig. 11.

Step2: The radial direction angle of channels is represented by the angle of the line connecting the center point of the bore and the centroid (average value of coordinates in that region) of the channel regions. Suppose the centroid of a channel is (x, y) and the center point of the bore is (x_c, y_c) , then the radial angle β of the channel could be calculated as equation (6). Fig. 12(a) shows the radial angle with the x-axis. Note that β is also an acute angle ranging from -90 to 90° .

$$\beta = \arctan \frac{y - y_c}{x_c - x} \quad (6)$$

Step 3: The angular separation γ between the radial line and the channel orientation reflects the deviation of the channel's direction to the radial direction. To avoid negative angle values or obtuse angle values, the angular separations are computed by equation (7). Fig. 12(b) shows the concept of angular separations.

$$\gamma = \begin{cases} |\alpha - \beta| & \text{if } |\alpha - \beta| \leq 90 \\ 180 - |\alpha - \beta| & \text{if } |\alpha - \beta| > 90 \end{cases} \quad (7)$$

Step 4: The circumferential channels' orientations are nearly perpendicular to the radial directions. So an angular separation threshold θ_T could be used to distinguish the radial channels from the circumferential channels, as indicated by equation (8).

$$\begin{cases} \text{channel } i \in \text{radial channels} & \text{if } \gamma_i < \theta_T \\ \text{channel } i \in \text{circumferential channels} & \text{if } \gamma_i \geq \theta_T \end{cases} \quad (8)$$

To demonstrate the channels classification algorithm more clearly, a

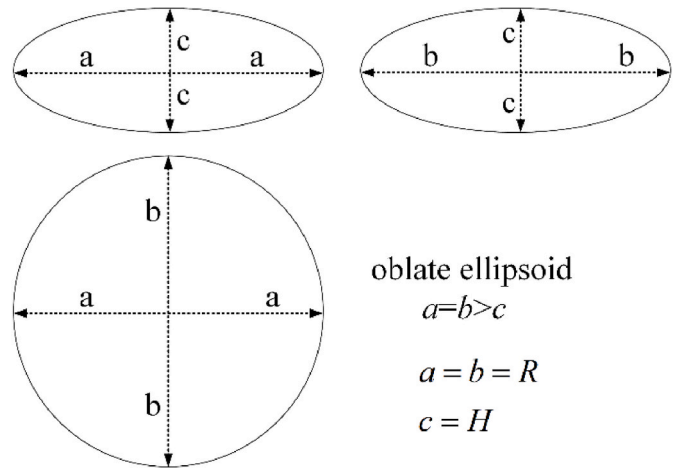


Fig. 19. Parameters of the oblate ellipsoid elements.

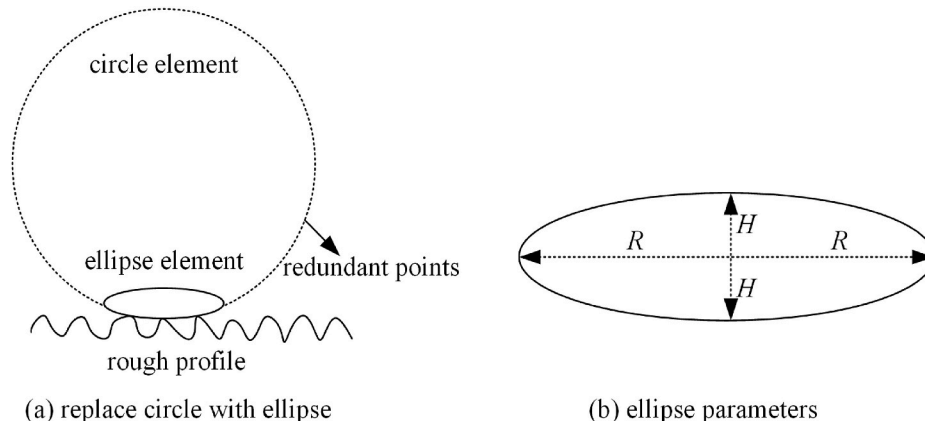


Fig. 18. The idea of replacing circle elements with ellipse elements.

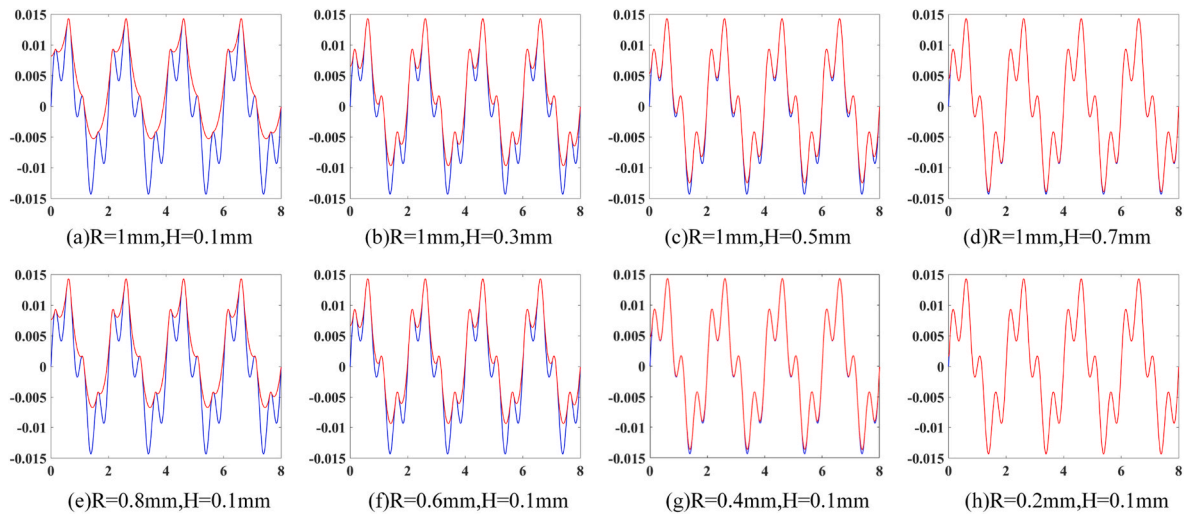


Fig. 20. Morphological closings using different sizes of ellipses.

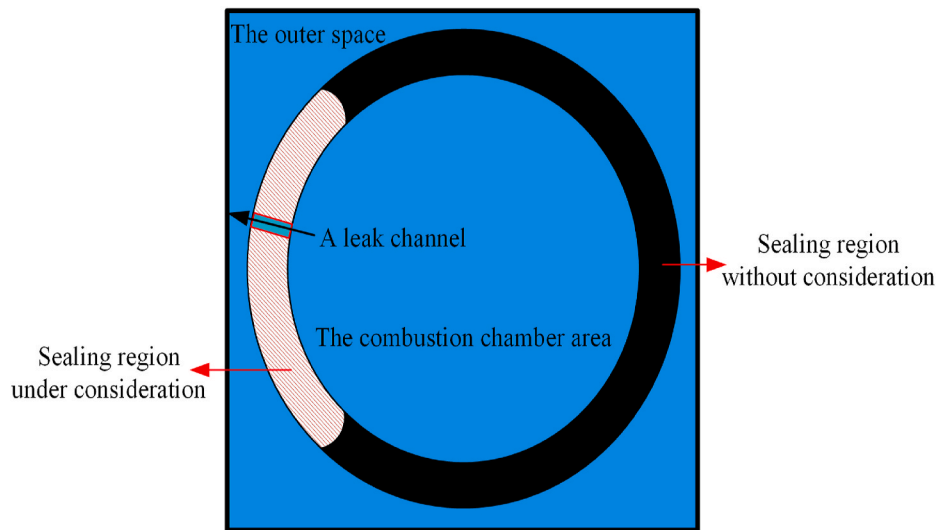


Fig. 21. The principle of detecting leakage by the area of connectivity classes.

simulated face-milled tool trajectory is tested. The point cloud of the face-milled surface is simulated according to equation (9). $H(R)$ sketches the profile of the tool along the radial direction. A point cloud of face-milled tool trajectories is simulated according to the tool profile shown in Fig. 13(a) with milling parameter $w = 136 \text{ rad/s}$, feed spacing $= 8\text{mm}/r$, and the point cloud is shown in Fig. 13(b).

$$\begin{cases} x = R \sin wt + ft \\ y = R \cos wt \\ z = H(R) \end{cases} \quad (9)$$

The ring-shaped region around the combustion chamber is a critical topography for sealing. A ring-shaped region is sampled from the simulated topography with an inner radius of 40 mm and an outer radius of 50 mm. Fig. 14(a) shows the topography of the sampled region, the periodic tool marks and grooves are dominant. Suppose the grooves with heights lower than 0.1 mm are potential leakage channels, with a simple global thresholding method, the potential leakage channels could be found. With a region labeling algorithm, the potential leakage channels are labeled and shown in Fig. 14(b). Following the proposed angle-based channels classification algorithm, the angular separations between channels' orientations and their radial directions could be calculated and shown in Fig. 15. From Fig. 15, it is clear that the angular separation

of circumferential channels is close to 90° , while the angular separation of radial channels is less than 70° . So the angle threshold θ_r could be set to be 80° , an appropriate value to distinguish circumferential channels from radial channels. The physical meaning of such a classification is that radial channels will connect the combustion chamber with outer spaces and they face high leakage risks, while the circumferential channels only connect outer spaces and won't cause gas leakage from combustion chambers.

Based on the analysis above, radial channels face significantly different leakage risks from circumferential channels. It is essential to divide the ring-shaped sealing region into different parts according to the channels' directions to study their leakage characteristics. For an isotropic surface topography, the leakage direction is along the radial direction. So radial lines connecting the chamber center with endpoints of the two longest circumferential channels are adopted as segmentation lines. The principle of radial segmentation is outlined in Fig. 16. The segmentation result of the sampled ring-shaped region from simulated topography in Section 2.2 is shown in Fig. 17. Channels in sub-regions R1 and R4 are circumferential, while channels in sub-regions R2 and R3 are radial.

Algorithm : $[flag, CAP] = \text{RegionIsLeak}(W, M, RM, SE)$

Input: ring shaped surface waviness W , ring shaped mask M , regional mask RM , structuring element SE

Output: $flag$, 1 for leakage and 0 for no leakage, CAP , contact area percentage

```

C = imclose(W,SE); contact = (C-W)>0
[m,n]=size(M); ME = zeros(m+2,n+2); ME(2:m+1,2:n+1)=M;
AME = regionprops(~ME,'Area'); BaseA = AME(1).Area+AME(2).Area;
Leak = ~M; Leak(RM)=contact(RM);
CAP=1-sum(contact(RM))/length(contact(RM));
LeakE = ones(m+2,n+2); LeakE(2:m+1,2:n+1)=Leak;
Larea = regionprops(LeakE,'Area');
If Larea(1).Area > BaseA
    flag =1
else
    flag = 0;
End if
    
```

Fig. 22. An algorithm to decide whether the considered region leaks or not.

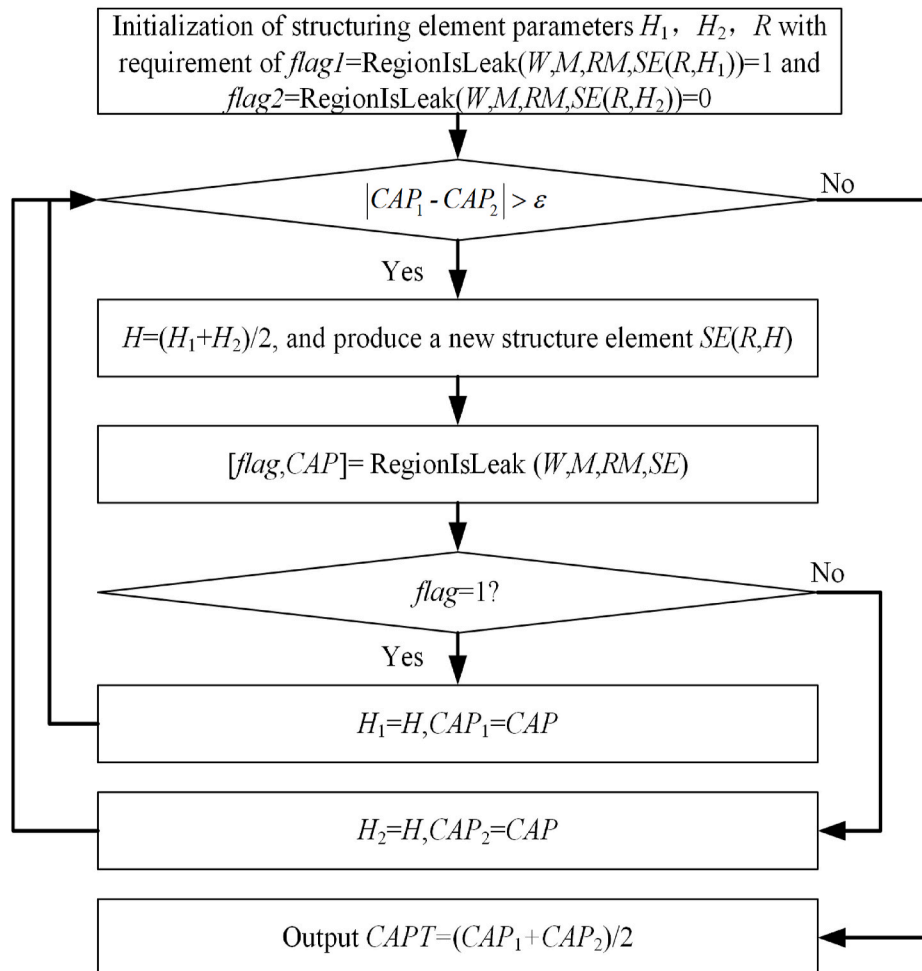


Fig. 23. The contact area percentage threshold searching algorithm.

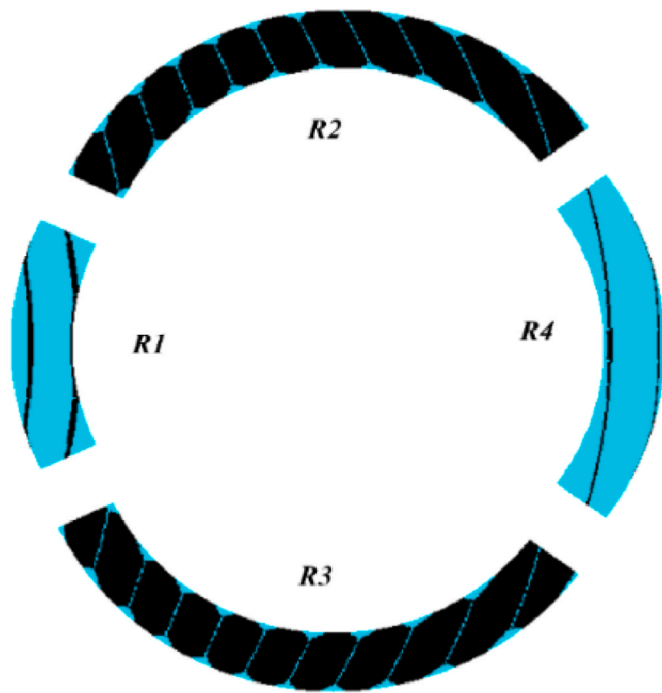


Fig. 24. The critical contact distribution of sub-regions on the simulated surface.

Table 1
CAPT values of the four sub-regions on the simulated surface.

Region	R1	R2	R3	R4
CAPT	0.12	0.91	0.91	0.07

2.3. Contact simulation and sealing analysis

Following sealing region segmentation is the sealing analysis by contact simulations. The MLS gaskets with coatings have complex compression-rebound characteristics. It is hard to calculate the contact behavior in this interface precisely. Malburg [19] provided another idea to simulate the contact behavior of conformable interfaces by implementing morphological closings on waviness profiles. And the extended three-dimensional virtual gasket method was detailed by Shao et al. [20]. However, the traditional circle structuring element used in profile filtering is very large (radius 5000 mm in Ref. [19]) and will face severe end effects and high computation costs. For measured surface topography, the horizontal range is usually much larger than the height range. The circle element has the same length in both directions and much

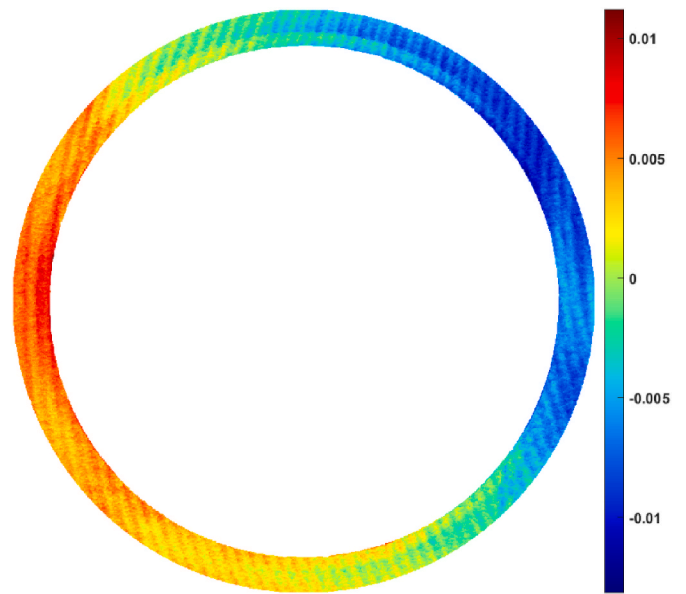
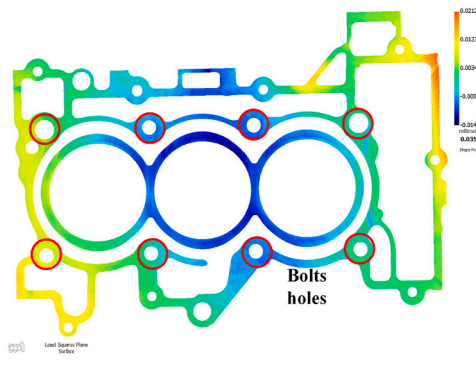


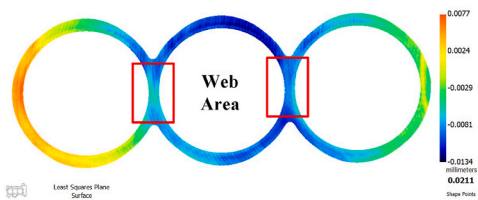
Fig. 26. A close view of the first ring-shaped sealing region.



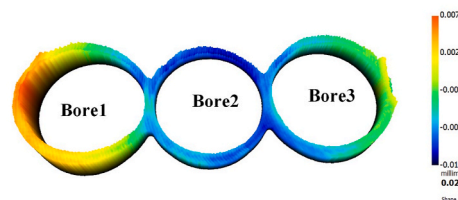
(a) Top surface of a cylinder block



(b) Two-dimensional view of the measured topography



(c) Two-dimensional view of surface topography around bores



(d) Three-dimensional view of surface topography around bores

Fig. 25. The cylinder block and its topography measurement results.

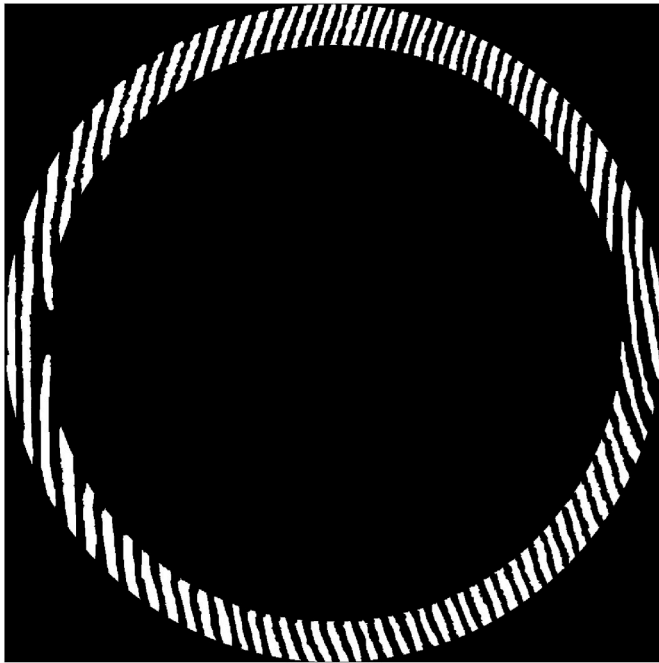


Fig. 27. A binary image indicating the potential leak channels.

redundancy exists in the height direction, as Fig. 18(a) shows. To solve this problem, an ellipse structuring element is proposed to accelerate the morphological operations and reduce the end effects. From Fig. 18(a), it is clear that a much smaller ellipse element could replace the large circle to do the same contact simulations without introducing redundant points. The ellipse parameters are shown in Fig. 18(b). By default, R represents the half-length of the major axis, while H is the half-length of the minor axis. Such thought could be extended to three-dimensional cases easily. And the ball element is substituted by an oblate ellipsoid element. And the ellipsoid parameters are shown in Fig. 19.

The contact area distribution in the interface between gaskets and surfaces of cylinder blocks or heads varies with the preload of bolts and combustion processes. A fixed structuring element cannot simulate the dynamic contact distributions. It is essential to develop a dynamic contact simulation method using different sizes of ellipsoid structuring elements. To explore the contact characteristics of different structuring elements, a simulated profile (see equation (10)) is tested. Morphological closings are performed on this profile with 8 different sizes of ellipses, and the closing profiles are shown with red lines in Fig. 20. The

original profiles are shown with blue lines. From Fig. 20(a) ~ (d), it could be seen that with the fixed length of the major axis, the larger length of the minor axis, the deeper the closing profiles could touch into the valleys. From Fig. 20(e) ~ (h), it could be found that with the fixed length of the minor axis, the shorter of the major axis, the deeper the closing profiles could touch into the valleys. This conclusion is also applicable to three-dimensional morphological closings with ellipsoid elements.

$$z = 0.01 \times (\sin(2\pi x / 2) + 0.5 \sin(2\pi x / 0.5)) \tag{10}$$

With the newly proposed ellipsoid elements, the contact distribution is determined by the waviness component (SW) with its morphological closing surface (SC). The contact surface $Contact$ could be viewed as a binary image with its definition as equation (11). And the contact area percentage (CAP) is defined as equation (12).

$$Contact = \begin{cases} 0 & SC(x, y) = SW(x, y) \quad \text{contact} \\ 1 & SC(x, y) > SW(x, y) \quad \text{no contact} \end{cases} \tag{11}$$

$$CAP = \sum_s [if (SC(x, y) = SW(x, y)) 1 \text{ else } 0] / S \tag{12}$$

Based on the contact surface definition, a connectivity-based leakage detection algorithm is proposed. The concept of surface connectivity could be reviewed in Ref. [21]. The 8-adjacency principle is adopted in this paper. If a leakage channel exists in the considered sealing region, the outer space will be connected with the combustion chamber area by this channel, as Fig. 21 shows. Then, the area of the biggest connectivity class will be greater than the summation of the outer space area and the combustion chamber area. The details of using such thought to decide whether leakage occurs or not are shown in Fig. 22 with pseudocodes.

With the leakage-deciding algorithm, it is possible to perform the dynamic sealing analysis. The most important variable to determine whether a surface will leak or not is the contact area percentage (CAP , defined by equation (12)). Persson and Yang [7] pointed that when two elastic solids of infinite size with randomly rough surfaces were squeezed together, a non-contact channel would percolate when the relative contact area was of the order 0.4, following percolation theory. However, real engineering surfaces are finite-sized and its topography has evident textures formed by machine tools. It is interesting to research the minimum contact area percentage required to form effective sealing on a real engineering surface with a fixed measurement resolution.

Different sizes of structuring elements could be viewed as different observation scales. By varying the sizes of structuring elements, the contact area distribution will change accordingly. A critical structuring

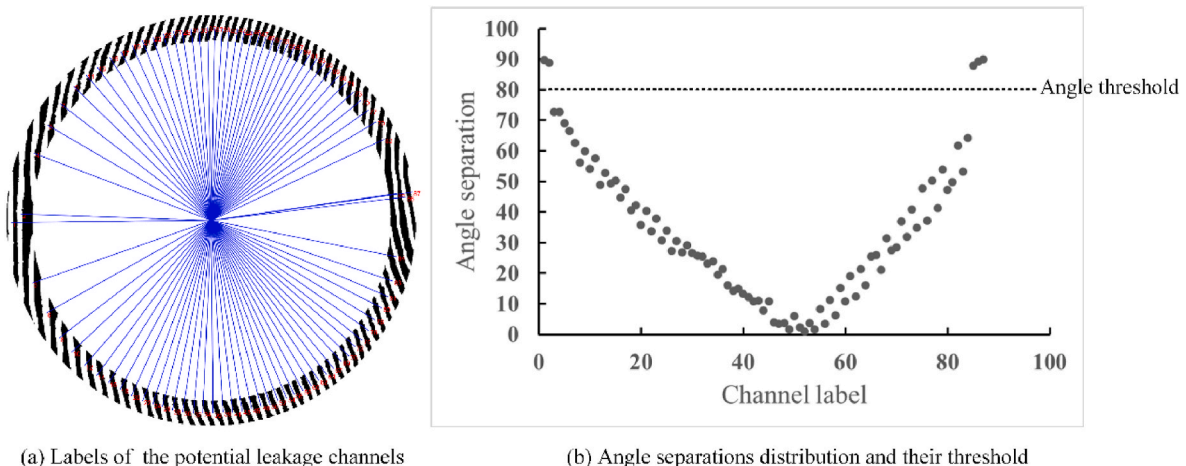


Fig. 28. The angle separations distribution of channels and their threshold.

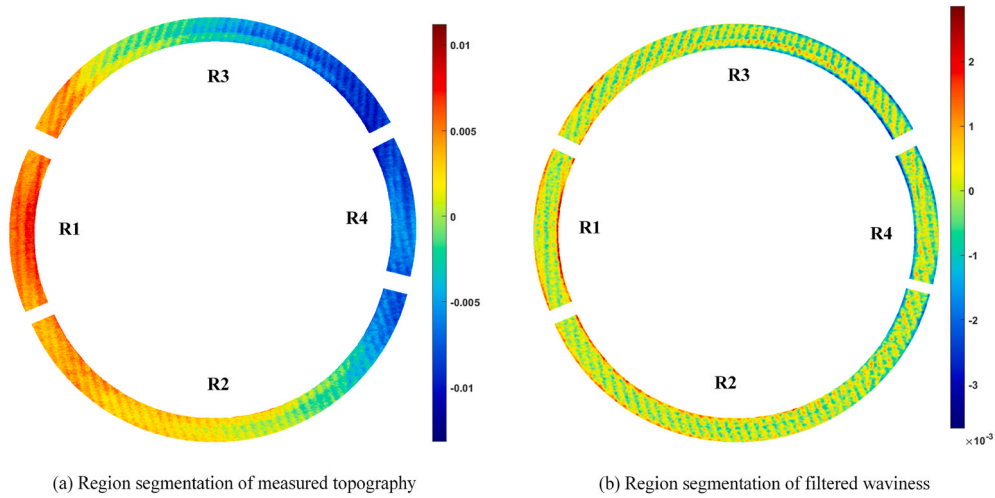


Fig. 29. Region segmentation on the measured topography and waviness.

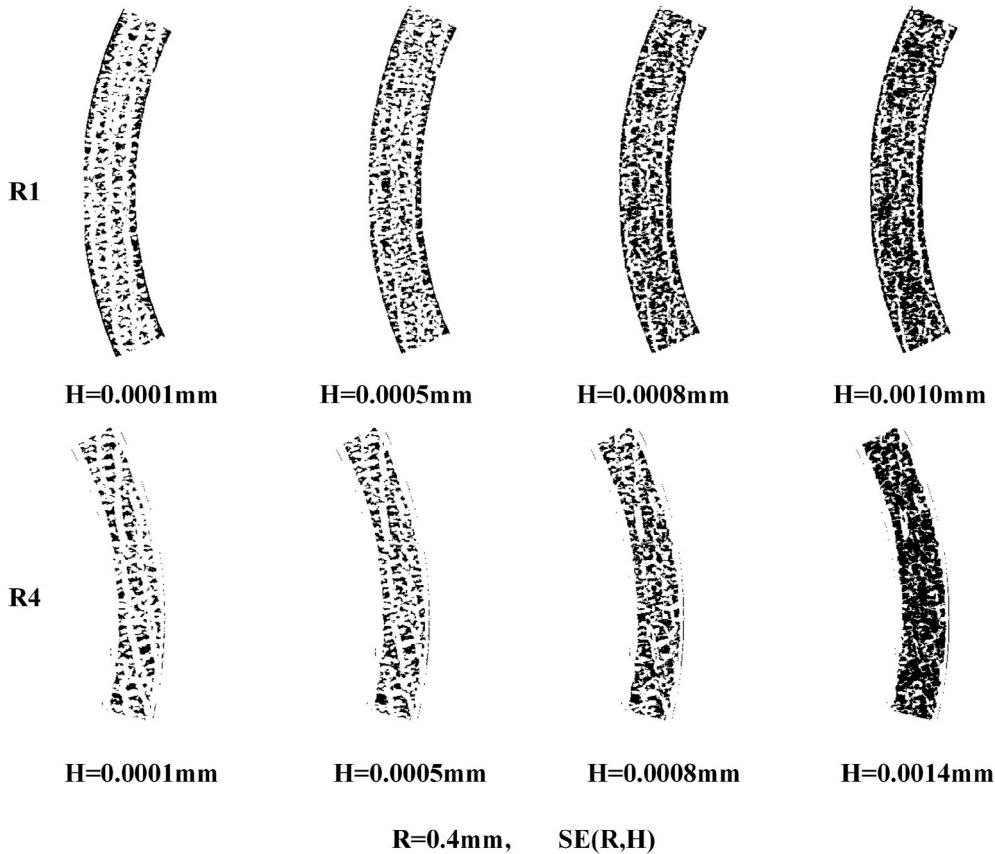


Fig. 30. The evolution processes of contact distribution of sub-regions R1 and R4.

element could be found by the proposed searching algorithm (shown in Fig. 23), and the corresponding CAPT (contact area percentage threshold) is the thresholding value to separate leakage from non-leakage situations.

Applying the CAPT searching algorithm to the simulated ring-shaped sealing region in Section 2.2, the critical contact distribution (least contact area to stop leakage) could be observed, as shown in Fig. 24. The black area indicates contact points, while the green area indicates non-contact points.

From Fig. 24, it is found that little contact area is required to stop leakage for circumferential channel regions, while radial channel

regions require much more contact area to form effective sealing. The CAPT values listed in Table 1 also support the conclusion above.

3. Case study

A cylinder block from an engine plant is studied to verify the effectiveness of the proposed sealing analysis method. The picture of the top surface of the cylinder block is shown in Fig. 25(a). It has only three bores and some material around the bores is removed to reduce the weight of the block, leaving a natural ring-shaped sealing region around the combustion chambers. The top surface was measured by ShaPix3D®

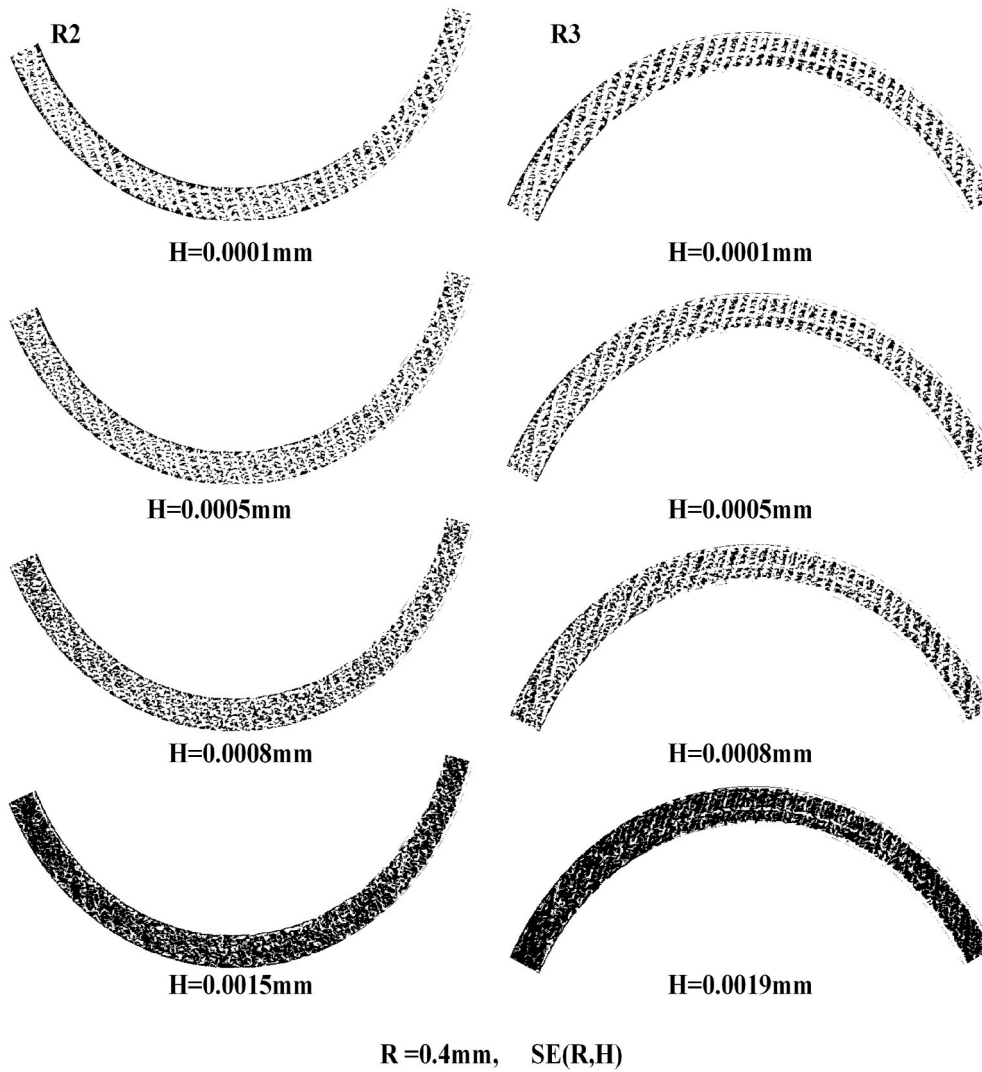


Fig. 31. The evolution processes of contact distributions of sub-regions R2 and R3

Table 2

CAPT values of the four sealing sub-regions.

Region	R1	R2	R3	R4
CAPT	0.55	0.67	0.73	0.56

1500 series (an HDM equipment as shown in Fig. 4), and the full view of the surface topography is shown in Fig. 25(b), with red circles outlining the locations of bolts holes. The lateral resolution and vertical resolution of Shapix3D are $80\mu\text{m}$ and $0.05\mu\text{m}$ respectively. The field of view is $150\text{mm} \times 150\text{mm}$, and the maximum number of points per view is 4

million. For a workpiece whose size exceeds the field of view, Shapix3D could stitch different point clouds from multiple views to generate the full view of the engineering surface. The three ring-shaped sealing regions around the combustion chambers are the critical topography for the sealing of combustion chambers. And the two-dimensional view and three-dimensional view of the ring-shaped regions are shown in Fig. 25 (c) and (d) respectively. The common sealing region between adjacent combustion chambers is called “web area”, as shown in Fig. 25(c) with red boxes. From left to right, the three bores are labeled with 1, 2 and 3 respectively, as shown in Fig. 25(d).

The sealing region around bore 1 is studied first. For a better inspection of the topography of this region, a close view of this ring-shaped

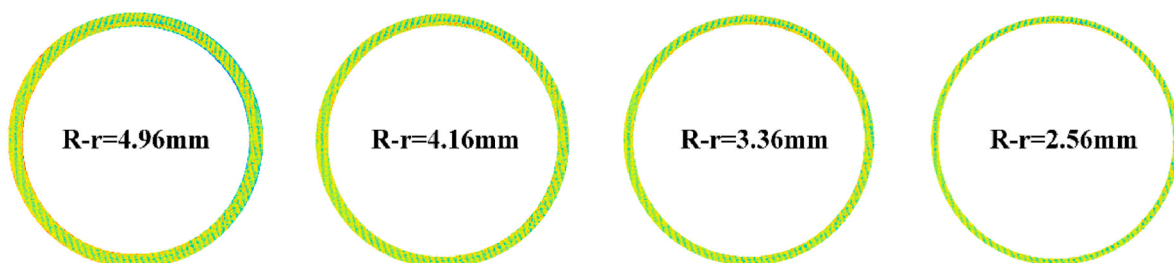


Fig. 32. Width reduced ring-shaped sealing regions.

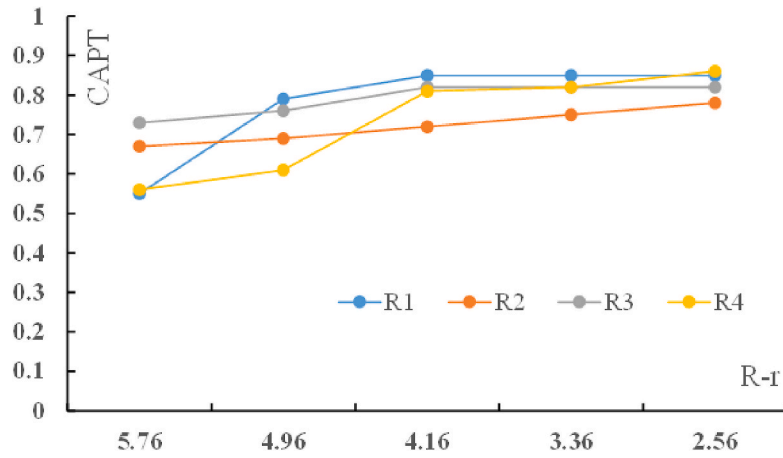


Fig. 33. CAPT values vary with the width of the ring-shaped region.

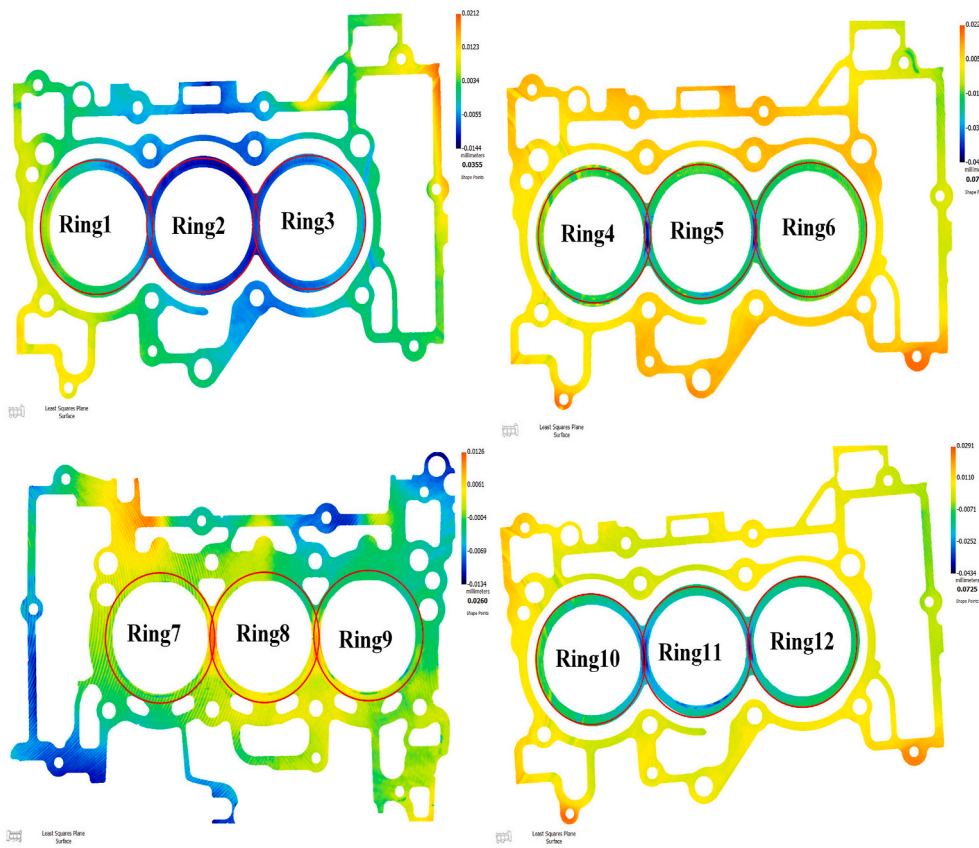


Fig. 34. 12 ring-shaped sealing regions.

topography is shown in Fig. 26. Tool paths could be seen from vision implicitly. Applying the tool paths reconstruction algorithm reviewed in Section 2.1 on the reversed topography of this region, a binary picture indicating the potential leak channels is obtained and shown in Fig. 27.

To distinguish circumferential channels from radial channels, the angle separation from the radial direction of each channel is computed and shown in Fig. 28. The label numbers and radial direction line of each channel are plotted in Fig. 28(a). The angle threshold of 80° separates circumferential channels from radial channels clearly, as shown in Fig. 28(b).

Using the region segmentation method proposed in Section 2.2, the segmentation results shown on measured surface topography and filtered waviness (areal spline filter with cut-off wavelengths of 0.8 mm

and 2.5 mm) are plotted in Fig. 29(a) and (b) respectively.

The dynamic sealing analysis is performed on the four waviness sub-regions with ellipsoid structuring element $SE(R, H)$. In this case, R is fixed as 0.4 mm, while H is changed continuously to simulate the contact distribution and search for the CAPT value. The evolution processes (from leakage to non-leakage) of contact distribution of sub-regions R1 and R4 (circumferential channels) are shown in Fig. 30. The white color indicates a non-contact area, while the black color indicates contact points. The last column shows the critical contact distribution, the least contact points required for non-leakage occurring.

For radial channel regions R2 and R3, their contact distribution evolution processes from leakage to non-leakage are demonstrated in Fig. 31. The last row shows the critical contact distribution, all leakage

Table 3
CAPT values of 12 ring-shaped sealing regions.

Sample	CAPT1	CAPT2	CAPT3	CAPT4
Ring 1	0.55	0.67	0.73	0.56
Ring 2	0.54	0.59	0.68	0.58
Ring 3	0.59	0.76	0.76	0.51
Ring 4	0.52	0.67	0.72	0.47
Ring 5	0.40	0.67	0.70	0.57
Ring 6	0.52	0.67	0.71	0.47
Ring 7	0.54	0.85	0.93	0.69
Ring 8	0.58	0.76	0.84	0.58
Ring 9	0.61	0.70	0.75	0.63
Ring 10	0.62	0.69	0.71	0.54
Ring 11	0.47	0.65	0.62	0.49
Ring 12	0.47	0.69	0.71	0.51

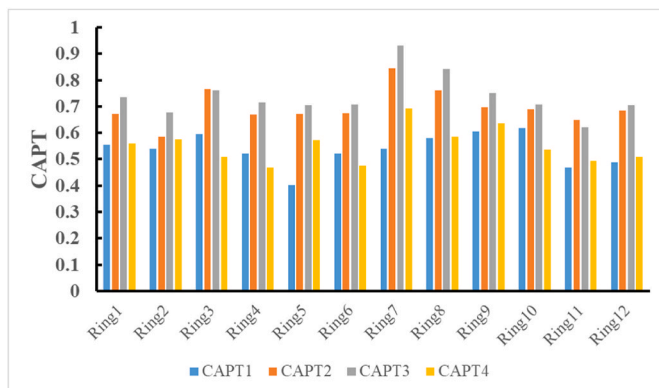


Fig. 35. CAPT values of each ring-shaped sealing region.

paths are blocked by contact points.

The CAPT value could be calculated from the critical contact distribution, and the CAPT values of the four sub-regions are listed in Table 2. The average CAPT of circumferential channel regions is about 0.56, while the average CAPT of radial channel regions is about 0.70, higher than circumferential channel regions. Compared with the simulated case in Section 2.3, the CAPT value of circumferential channel regions is much higher in real engineering surfaces. Because of the irregularities of real surface topography, circumferential tool marks are broken and there are more microchannels to link the outer space with the inner space through circumferential channels. For radial channel regions, the CAPT values of real engineering surfaces are lower than the simulated surface, since the radial channels are more easily blocked on real engineering surfaces due to tool wear and other machining errors. Compared with Persson's theory [7], the critical contact area percentage of the face-milled surface is higher than the theoretical value (0.4). The reason behind this is the face-milled surface topography doesn't match the hypothesis of fractal and isotropic surface micro-geometry in Persson's theory. The texture directions or tool paths' directions do have a significant impact on the surface's sealing properties. And generally, circumferential textures are advantageous for surface sealing, while radial textures are prone to leakage. The good news is that the sealing regions of circumferential channels are almost overlapped with the web area between adjacent combustion chambers, as indicated by Fig. 25(c). In other words, the web area could achieve effective sealing with less contact pressure than other regions of radial channels. This result also agrees with the distribution of bolts. Since bolts are usually distributed as Fig. 25(b) shows, the web areas are far away from bolts, the torque pressure assigned to the web areas is less than other regions. The circumferential channels in the web area are advantageous for forming effective sealing under relatively low contact pressure.

The width of the ring-shaped region $R-r$ (R is the radius of the outer circle while r is the radius of the inner circle) also impacts the CAPT

value of the sealing regions. The ring width $R-r$ in Fig. 26 is 5.76 mm. Four widths reduced ring-shaped sealing regions' waviness are shown in Fig. 32. The CAPT values computed with the same segmentation lines (still four sealing sub-regions R1~R4) on the ring-shaped sealing regions with different widths are plotted in Fig. 33. As the width of rings decreases, the CAPT value increases. This trend implies that for the narrower ring-shaped sealing regions, there needs more percentage of contact area to form effective sealing. The extreme case is the line sealing, only 100% contact area percentage could stop leakage from occurring. For gasket design, the width of the beads around the combustion chambers is a key design variable. From the analysis above, it is recommended that the design width of the bead should be wider enough to cover at least one complete circumferential channel. Such width could stop gas leakage between adjacent bores with a relatively low contact area percentage.

To verify the influence of channels' directions on CAPT values of sealing regions, 12 ring-shaped sealing regions were extracted from 3 top surfaces of cylinder blocks and 1 bottom surface of a cylinder head. The topography of the four surfaces and the 12 ring-shaped sealing regions (denoted as Ring1 to Ring12) are shown in Fig. 34. Repeat the analysis procedures above, each sealing region is divided into 2 circumferential channel regions (R1 and R3) and 2 radial channel regions (R2 and R4), and the corresponding CAPT values are calculated and listed in Table 3. The CAPT value of region R_i is denoted as CAPT $_i$. Fig. 35 shows the bar graph of the CAPT values of the 12 ring-shaped regions. And it is clear that $\min(\text{CAPT}_2, \text{CAPT}_3) > \max(\text{CAPT}_1, \text{CAPT}_4)$ holds for every ring-shaped sealing region. Averagely, the circumferential channel regions require 54% area contact to form effective sealing, while the radial channel regions require 72% area contact to stop leakage. This result strongly supports the conclusion that circumferential channels or paths are advantageous for surface sealing, while radial channels are prone to leakage.

The analysis of all real surfaces was carried out with MATLAB R2020a on a desktop computer with 8 GB RAM and 3.60 GHz i7-7700 CPU. The average running time of the analysis for a single ring-shaped sealing region is 44.67s. The proposed methodology is applicable for all engineering surfaces machined by face-milling with disc milling cutters. Especially, the contact simulation and sealing analysis method (Module 3) is applicable for all kinds of engineering surfaces sealed with conformable gaskets.

4. Conclusion

This paper proposed a sealing analysis method for face-milled surfaces. First, the tool paths are reconstructed by the newly proposed surface segmentation methodology. Then the ring-shaped sealing region is divided into four sub-regions according to their channels' directions. An angle separation calculation method is proposed and a threshold value is found to distinguish circumferential channels from radial channels. An ellipsoid structuring element is proposed to simulate the contact behavior between rough surfaces and gaskets by morphological closings. A contact area percentage threshold (CAPT) searching algorithm is proposed to find the minimum contact area percentage required to block leakage channels.

By real case studies, it is found that channels' directions do have a significant impact on surfaces' sealing properties. Circumferential channels or paths are advantageous for surface sealing, while radial channels are prone to leakage. The width of the ring-shaped sealing region also has an impact on its CAPT value. The narrower the ring-shaped sealing region, the higher the contact area percentage it requires to form effective sealing. The cylinder head gasket design optimization based on the sealing analysis of surface topographies will be the next research topic. And in the future, more experimental work will be conducted to verify the predicted contact states and promote the sealing efficiency of MLS gaskets.

Declaration of competing interest

The authors declare that they have no known competing financial interests or personal relationships that could have appeared to influence the work reported in this paper.

Acknowledgements

This work was supported by the National Natural Science Foundation of China (Grant No. 51775343 and No. 51535007).

References

- [1] Flitney R. In: Flitney R, editor. Chapter 2 - static seals," seals and sealing handbook. fifth ed. Oxford: Elsevier Science; 2007. p. 7–104.
- [2] Cierocki K, Ermert T. Topographic stopper for cylinder head gaskets. *Mtz Worldwide* 2003;64(1):9–12.
- [3] Kestly M, Unseld G, Weiss A, Ludwig J. MLS cylinder head gasket wave stopper. 2003. SAE Technical Paper 2003-01-0474.
- [4] Katsurai T, Adachi K, Nishiyama T, Murakami O. Cylinder head gasket for high combustion pressure diesel engines. *SAE International Journal of Engines* 2009;2(1):941–7.
- [5] Capretta R, Ohigashi H. Design methodology for automotive multi-layer steel cylinder head gaskets. 1995. SAE Technical Paper-950322.
- [6] Ma Z, Yu T, Xing Y, Liu L, Hu M, A method for studying the sealing performance of cylinder head matched surface, *RICAI 2020: 2020 2nd International Conference on Robotics, Intelligent Control and Artificial Intelligence*.
- [7] Persson BNJ, Yang C. Theory of the leak-rate of seals. *J Phys Condens Matter* 2008; 20(31):315011.
- [8] Aharony A, Stauffer D. Introduction to percolation theory. London: Taylor&Francis; 2003.
- [9] Persson BNJ, Albohr O, Creton C, Peveri V. Contact area between a viscoelastic solid and a hard, randomly rough, substrate. *J Chem Phys* 2004;120(18):8779–93.
- [10] Bottiglione F, Carbone G, Mangialardi L, Mantriota G. Leakage mechanism in flat seals. *J Appl Phys* 2009;106(10):104902.
- [11] Bottiglione F, Carbone G, Mantriota G. Fluid leakage in seals: an approach based on percolation theory. *Tribol Int* 2009;42(5):731–7.
- [12] Lorenz B, Persson BNJ. Leak rate of seals: effective-medium theory and comparison with experiment. *European Physical Journal E* 2010;31(2):159–67.
- [13] Pérez-Ráfols F, Larsson R, Almqvist A. Modelling of leakage on metal-to-metal seals. *Tribol Int* 2016;94:421–7.
- [14] Lorenz B, Persson BNJ. On the dependence of the leak rate of seals on the skewness of the surface height probability distribution. *Epl* 2010;90(3).
- [15] Ledoux Y, Lasseux D, Favreliere H, Samper S, Grandjean J. On the dependence of static flat seal efficiency to surface defects. *Int J Pres Ves Pip* 2011;88(11–12): 518–29.
- [16] Hao MM, Wang YL, Li ZT, Sun XH. Effects of surface topography on hydrodynamic performance of liquid film seals considering cavitation. *Ind Lubric Tribol* 2018;70(6):984–92.
- [17] Liu S, Jin S, Zhang X, Wang L, Mei B, Hu B, Controlling topography of machined surface for adhesive-sealing, ASME 2017 12th international manufacturing science and engineering conference collocated with the JSME/ASME 2017 6th international conference on materials and processing.
- [18] Zhang F, Liu J, Ding X, Yang Z. An approach to calculate leak channels and leak rates between metallic sealing surfaces. *J Tribol* 2016;139(1):011708.
- [19] Malburg MC. Surface profile Analysis for conformable interfaces. *Journal of Manufacturing Science and Engineering, Transactions of the ASME* 2003;125(3): 624–7.
- [20] Shao YP, Yin YX, Du SC, Xia TB, Xi LF. Leakage monitoring in static sealing interface based on three dimensional surface topography indicator. *Journal of Manufacturing Science and Engineering, Transactions of the ASME* 2018;140: 101003.
- [21] Shao YP, Yin YX, Du SC, Xi LF. A surface connectivity based approach for leakage channel prediction in static sealing interface. *J Tribol* 2019;141(6):062201.
- [22] Deltombe R, Bigerelle M, Jourani A. Analysis of the effects of different machining processes on sealing using multiscale topography. *Surf Topogr Metrol Prop* 2015;4(1):015003.
- [23] Yang Z, Liu J, Ding X, Zhang F. The effect of anisotropy on the percolation threshold of sealing surfaces. *J Tribol* 2018;141(2):022203.
- [24] Liao C, Xu X, Fang H, Wang H, Man M. A leakage model of metallic static seals based on micromorphology characteristics of turning flange surface. *Ind Lubric Tribol* 2015;67(6):572–81.
- [25] Robbe-Valloire F, Prat M. A model for face-turned surface microgeometry application to the analysis of metallic static seals. *Wear* 2008;264(11–12):980–9.
- [26] Du SC, Liu CP, Huang DL. A shearlet-based separation method of 3D engineering surface using high definition metrology. *Precis Eng* 2015;40:55–73.
- [27] Wang M, Xi LF, Du SC. 3D surface form error evaluation using high definition metrology. *Precis Eng* 2014;38(1):230–6.
- [28] Yin Y, Shao Y, Wang K, Du S, Xi L. Segmentation of workpiece surfaces with tool marks based on high definition metrology. *J Manuf Process* 2020;57:268–87.
- [29] Ren J, Park C, Wang H. Stochastic modeling and diagnosis of leak areas for surface assembly. *Journal of Manufacturing Science and Engineering, Transactions of the ASME* 2018;140(4):041011.
- [30] Du Shichang, Xi Lifeng. High definition metrology based surface quality control and applications. Singapore: Springer; 2019.